Mesoporous silica nanoparticles functionalized with a dialkoxide diorganotin(IV) compound: In search of more selective systems against cancer cells

Diana Díaz-García[a], Lucia Sommerova[b], Andrea Martisova[b], Hana Skoupilova[b], Sanjiv Prashar[a], Tomas Vaculovic[c], Viktor Kanicky[c], Isabel del Hierro [a], Roman Hrstka[b,*] and Santiago Gómez-Ruiz[a,*]

[a] *COMET-NANO Group, Dpto. de Biología y Geología, Física y Química Inorgánica, ESCET, Universidad Rey Juan Carlos, Spain.*

[b] *Masaryk Memorial Cancer Institute, Regional Centre for Applied Molecular Oncology, Zluty kopec 7, 65653 Brno, Czech Republic.*

[c] *Dpt. of Chemistry, Faculty of Science, Masaryk University, Kamenice 5, 62500 Brno, Czech Republic*

* Corresponding authors: R. Hrstka (hrstka@mou.cz)

S. Gómez-Ruiz (santiago.gomez@urjc.es)

Abstract:

Mesoporous silica nanoparticles (MSN) have been functionalized with the polyamino ligand N^1-(3-trimethoxysilylpropyl)diethylenetriamine to give the material MSN-DETATMS (**M1**). The reaction of **M1** with the diphenyltin(IV) compound **Sn1** [obtained previously from the reaction of (3-glycidyloxypropyl)trimethoxysilane and diphenyltin(IV) dichloride in the presence of two equivalents of sodium hydroxide] in a quantity to obtain a theoretical 10% wt Sn/SiO_2, gave the material MSN-DETATMS-O_2-$SnPh_2$ (**M2**). Alternatively, **M1** was reacted with folic acid to achieve the incorporation of the folate fragment via formation of an amido bond MSN-DETATMS-FA (**M3**) and subsequently with **Sn1** to give the tin-functionalized material MSN-DETATMS-FA-O_2-$SnPh_2$ (**M4**). **M1**–**M4** have been characterized by several methods such as infrared spectroscopy (FT-IR), powder X-ray diffraction (XRD), X-ray fluorescence (XRF), solid-state NMR spectroscopy, nitrogen adsorption-desorption isotherms, electrochemical methods, scanning electron microscopy (SEM) and transmission electron microscopy (TEM). All the synthesized nanomaterials have been tested *in vitro* against a wide variety of cancer and non-cancer cells in order to determine different aspects of their antitumour effects such as cell uptake, cell death, cell migration and cell invasion, to observe whether the incorporation of folate fragments may increase the cell uptake and selectivity towards cancer cells, thus increasing their potential applicability in future chemotherapeutic approaches.

Keywords: organotin(IV); anticancer; mesoporous silica nanoparticles; cytotoxicity; folic acid; cell migration; cell invasion

1. Introduction

Cancer is one of the leading causes of death in the world with about 9.6 million fatalities in 2018 [1]. The incidence of cancer is expected to dramatically increase from 18.1 million cases declared in 2018 to *ca.* 29.5 million cases in 2040 [2]. Therefore, intensive research is needed to discover more active and selective anticancer chemotherapeutic agents, which administered in lower doses, present less aggressive side effects and help to reduce the number of cancer deaths worldwide.

In the context of chemotherapy, metal-based drugs, especially those based on platinum [3,4], have for more than 40 years successfully treated a wide number of tumours [5]. However, from a basic point of view, metallodrugs present problems associated with their low stability in physiologic media, active species transformations, low solubility in aqueous systems and a low degree of internalization in cells leading to limited targeting [6]. All this means the success rate of metallodrugs in therapies remains limited, due to inefficient drug accessibility to the tumour tissue, the development of multi-drug resistance and the dynamic heterogeneous biology of the growing tumours. Therefore, one of the most important active research topics in this field is the search of innovative technologies for controlled targeted metallodrug-delivery and smart release to eradicate tumour cells while sparing non-tumourigenic cells [6,7].

One of the most interesting approaches for obtaining more selective metallodrug-functionalized systems is the use of nanostructured silica-based materials, which have recently been considered very interesting scaffolds for the development of drug delivery systems to direct the drug to the cancer cells. Since our pioneering study published in 2009 in which titanium-metallodrugs were supported onto nanostructured silica (MCM-41 and SBA-15) [8], several alternative systems based on different nanostructured materials as vectors for metallodrugs have been used for the protection and delivery of the metal-containing therapeutic agent to the biological target in cells leading to its more effective administration [6,7,9].

The studies of this kind of systems have demonstrated that metallodrug-functionalized silica-based nanomaterials usually work as "non-classical" drug-delivery nanosystems as they do not release to the medium the metal-based drug, but in most cases they act as entire nanoparticulated therapeutic systems, presumably through the action of the supported metallodrug on the silica particles [10–20]. These studies have shown that the silica-based nanostructured systems are more cytotoxic than the free metallodrugs because of a higher uptake of silica particles by the cancer cells due to the enhanced permeability and retention (EPR) effect of malignant cells, most probably because they improve the effectiveness in transport processes [14,19]. In addition, they induce programmed cell death in tumour cell populations by impairing the damaged DNA repair mechanisms and by upregulation of intrinsic and extrinsic apoptotic signalling pathways [14], to trigger apoptosis by interfering with the TNF-α pathway [17,18] or through the Fas-FasL system depending on the supported metallodrug [18]. Thus, a simple change in the design of the nanostructured material has a strong influence on the metabolic activity of the tumour cells, which modulates the apoptotic pathways by different mechanisms.

The majority of studies with nanostructured silica-based materials functionalized with metallodrugs have focused on different metal complexes of titanium [8,10–12,14,15,17,18], tin [13,16,18,21,22] and copper [23]. A very strong therapeutic potential of tetraorganotin(IV)-supported systems was observed. They were able to almost completely eradicate B16 melanoma tumour growth in syngeneic C57BL/6 mice by the induction of cell differentiation to a non-invasive phenotype [13] among other interesting properties attributed, especially, to the functionalized SBA-15 materials [16,21,22].

In general, one of the most important aspects of mesoporous silica to promote a significant increase of the cytotoxic activity is both the protection of the active species, which usually increases the bioavailability of the drug inside the cells [24,25], and the capacity to load a high quality of drug giving a controlled and vectorised release in the affected area [6]. Thus, in view of the therapeutic potential of these systems, and that one of their most limiting aspects is the low degree of cell uptake, we decided to explore in detail the potential application of tin-

functionalized mesoporous silica nanoparticles (below 100 nm size) by including folate fragments. The folate receptor is a recognised biomarker for tumour cells due to its overexpression relative to normal cells, and since its absolute level of expression on cancer cells should be sufficient to enable the delivery of therapeutic quantities of the desired drug [26].

Indeed, only during the last year a wide variety of systems such as for example liposomes [27], biocompatible polymers [28] and other nanomaterials [29] have been functionalized with folic acid in order to improve their therapeutic potential against a wide variety of cancerous systems such as mammalian cells 4T1 or MCF-7 and other malignant colonies based on HeLa or Hep G2. In this context, the incorporation of folate fragments for the enhancement of the therapeutic selectivity of silica-based systems has already been studied in different particles. For example, in the case of nanobubbles of silica the incorporation of folic acid and a chitosan derivative led to intracellular explosion of cancer cell lines of different origins [30]. On the other hand, the incorporation of folate fragments in mesoporous silica nanoparticles led to a slight increase of the selectivity towards cancer cells compared with systems without the folate fragments in the delivery of typical anticancer drugs such as topotecan [31], thymoquinone and melatonin [32], dacarbazine [33], docetaxel [34], vinblastine [35], camptothecin [36] or doxorubicin [37]. In addition, a similar behaviour has been observed when studying the delivery of natural products with antitumoral properties such as curcumin [38].

In this context, although the strategy of including folate fragments in mesoporous silica systems has been utilized regularly, the number of reports regarding the incorporation of folate fragments in metallodrug-functionalized mesoporous silica nanomaterials is still scarce, as these systems have only been studied with therapeutic gold(III) compounds [39]. Therefore, considering that the incorporation of the folate fragments in mesoporous silica nanoparticles functionalized with tin(IV) alkoxide-based metallodrugs has not been studied yet, we designed this work to determine if this could be a good strategy to increase the cell uptake and selectivity towards different cancer cell lines, thus increasing their potential applicability in future chemotherapeutic actions.

2. Experimental section
2.1. General remarks on the synthesis and characterization of the materials

All functionalization reactions were performed using standard Schlenk tube techniques in an atmosphere of dry nitrogen, except those of the synthesis of the starting material MSN and the EDAC coupling to synthesize material **M3**. Solvents were distilled from the appropriate drying agents and degassed before use. The reagents used in the preparation of the starting material (MSN), namely, tetraethyl orthosilicate (TEOS, Sigma Aldrich) and hexadecyltrimethylammonium bromide (CTAB, Acros Organics) and sodium hydroxide (NaOH, Scharlau) were used as received, without further purification. The reagents used for the functionalization reactions, namely, N[1]-(3-trimethoxysilylpropyl)diethylenetriamine (DETATMS, Fluorochem Ltd), (3-glycidyloxypropyl)trimethoxysilane and diphenyltin(IV) dichloride, MES monohydrate, N-(3-dimethylaminopropyl)-N'-ethylcarbodiimide (EDAC), N-hydroxysuccinamide (NHS), 2-mercaptoethanol, hydroxylamine hydrochloride and folic acid (FA) were purchased from Sigma Aldrich and used directly without further purification.

[13]C-CP MAS spectra were recorded on a Varian-Infinity Plus Spectrometer at 400 MHz operating at 100.52 MHz proton frequency (4 μs 90° pulse, 4000 transients, spinning speed of 6 MHz, contact time 3 ms, pulse delay 1.5 s). X-ray diffraction (XRD) pattern of the systems were obtained on a Philips Diffractometer model PW3040/00 X'Pert MPD/MRD at 45 kV and 40 mA, using a wavelength Cu Kα (λ = 1.5418 Å). Sn wt% determination by X-ray fluorescence was carried out with an X-ray fluorescence spectrophotometer Philips MagiX with a X-ray source of 1 kW and a Rh anode using a helium atmosphere. FT-IR analysis was determined with a Termo Nicolet Avatar 380 FT-IR spectrometer with a Michelson type filter interferometer N_2 gas adsorption–desorption isotherms were performed using a Micromeritics ASAP 2020 analyzer.

Conventional transmission electron microscopy (TEM) was carried out on a JEOL JEM 1010, operating at 100 kV.

## 2.2. Synthesis of mesoporous silica nanoparticle (MSN)

The synthesis of MSN was carried out with a slight modification of the experimental procedure reported by Zhao *et al* [40]. An aqueous solution of CTAB (1.00 g, 2.74 mmol) was prepared in 480 mL of Milli-Q water, subsequently, sodium hydroxide (2 M, 3.5 mL) was then added to the solution and the temperature increased to 80 ºC. Afterwards, the silica precursor TEOS (5 mL, 22.4 mmol) was added dropwise under vigorous stirring and the mixture allowed to react for 2 additional hours. The white precipitate was isolated by filtration and washed with abundant Milli-Q water and with methanol (2 × 20 mL) and dried for 24 hours at 80 ºC in a stove. Finally, a calcination process at 500 ºC was carried out for 24 hours with an increasing temperature ramp of 1 ºC/min.

2.3. Functionalization of MSN-DETATMS (M1)

The functionalization of MSN was carried out using similar procedures described previously by our group [24,25]. In summary, MSN (1.00 g) was partially dehydrated under vacuum at 80 ºC for 24 hours and suspended in 20 mL of dry toluene. The mixture was then treated with a solution of N^1-(3-trimethoxysilylpropyl)diethylenetriamine (1.94 mL, 7.53 mmol) in 30 mL of dry toluene. The mixture was stirred for 48 hours at 110 ºC, and then filtered to isolate the precipitate, which was washed with toluene and diethylether and subsequently dried for 24 hours at 80 ºC.

2.4. Synthesis of MSN-DETATMS-O$_2$-SnPh$_2$ (M2)

Firstly, the tin compound **Sn1** (Scheme 1) was synthesized by the reaction of (3-glycidyloxypropyl)trimethoxysilane and SnPh$_2$Cl$_2$ in the presence of two equivalents of NaOH. In summary, 103.4 µL (0.468 mmol) of (3-glycidyloxypropyl)trimethoxysilane was dissolved in 20 mL of methanol and then sodium hydroxide (0.468 mL of a 2.0M solution in water) was added for the epoxide opening reaction. The solution was stirred for 60 minutes at room temperature (r.t.) and, subsequently, a solution of SnPh$_2$Cl$_2$ (160.9 mg, 0.468 mmol to obtain a theoretical level of 10 % Sn/SiO$_2$ in the following reaction with MSN-based materials) in 10 mL of methanol was added dropwise and the mixture was stirred for 24 hours at 60 ºC. After this time, the mixture was filtered under a nitrogen atmosphere with a filter cannula to eliminate NaCl. The filtrate was added to a suspension of 0.5 g of **M1** in 10 mL of methanol, and the mixture was stirred for 24 hours at 60 ºC. The mixture was then centrifuged and the solid obtained washed with methanol and Milli-Q water. Finally, the resulting solid was dried in a stove at 80 ºC for 24 hours.
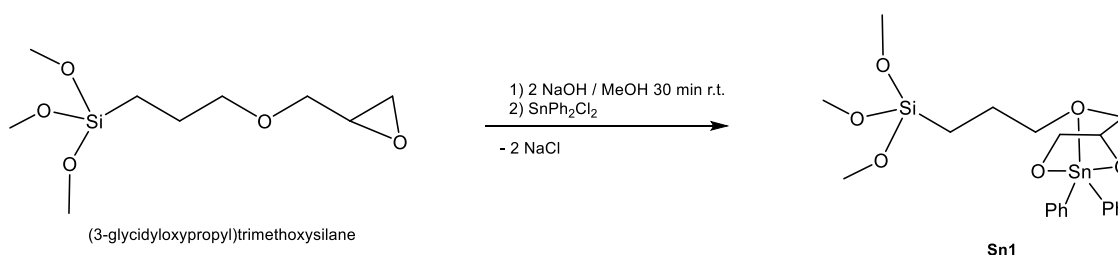
Scheme 1. Synthesis of the tin complex **Sn1**

2.5. Synthesis of MSN-DETATMS-FA (M3)

For the functionalization of MSN-DETATMS with folic acid, an EDAC coupling reaction was carried out. For this, 50 mL 0.1 M of MES Buffer was prepared with 0.5 M sodium chloride. Subsequently, 50 mg of folic acid (10% functionalization of **M1**) was dissolved in 12.5 mL of DMSO (in an ultrasound bath) and this solution was added to the MES buffer solution containing 20 mg (0.104 mmol) of EDAC and 30 mg (0.261 mmol) of NHS. The mixture was allowed to react

under vigorous stirring for 15 minutes at room temperature. Subsequently, 0.5 g of MSN-DETATMS was added to the EDAC solution and allowed to react for 2 hours at room temperature under stirring and then 7 µL (0.107 mmol) of 2-mercaptoethanol was added to the solution and stirred for additional 30 minutes. Finally, 41.5 mg (0.597 mmol) of hydroxylamine was added to quench the reaction. The mixture was then centrifuged (6000 rpm, 10 minutes) and washed with DMSO, ethanol, water and diethylether (1 × 10 mL each) in order to remove the excess of reagents. The product was dried in a stove at 80 ºC overnight.

2.6. Synthesis of MSN-DETATMS-FA-O$_2$-SnPh$_2$ (M4)

The synthesis of material **M4**, was carried out following an identical procedure to that described for **M2** (Section 2.4); 103.4 µL (0.468 mmol) of (3-glycidyloxypropyl)trimethoxysilane, sodium hydroxide (0.468 mL of a 2.0M solution in water), 160.9 mg (0.468 mmol) of SnPh$_2$Cl$_2$ and 0.5 g of **M3**.

2.7. Characterization by electrochemical techniques

The modified carbon paste electrodes (MCPE) used as working electrode were prepared by mixing with a pestle in an agate mortar the previously modified mesoporous silica nanoparticles with graphite (Metrohm) (6-10% (w,w) ratio) and mineral oil as agglutinant (Sigma-Aldrich) until a uniform paste was obtained. The resulting material was packed into the end of a Teflon cylindrical tube equipped with a screwing stainless steel piston providing an inner electrical contact. All of the initial electrode activity could always be restored by simply removing the outer layer of paste by treatment with polishing paper. DPV parameters were as follows: initial potential of 0.0 V, end potential -1.5 V, modulation time 0.057 s, time interval 0.2 s, step potential 1.05 mV/s and modulation amplitude 75 mV.

### 2.8. Human cancer cell lines and their cellular uptake

Lung cancer derived A549 cells, breast cancer derived MDA-MB-231 cells and embryonic kidney HEK 293 cells were cultured in high glucose D-MEM medium (Sigma-Aldrich). Ovarian cancer cell line SK-OV-3 was maintained in McCoy's 5A (Sigma-Aldrich). Both media were supplemented with 10% fetal bovine serum (Biochrom), 100 U/ml penicillin, 0.1 mg/ml streptomycin (Hyclone Laboratories) and 2 mM L-glutamine (Gibco) in a humidified incubator at 37 °C in 5% CO$_2$ atmosphere. To study cellular uptake, the cells were seeded on a 10 cm plate in the confluence ~70% and the next day exposed to 10 µg/ml of **M1**-**M4** for 24 hours. Then the cells were harvested, washed twice with PBS, counted using CASY Model TT Cell Counter (Roche) and resulting cell pellets with the same number of cells were frozen at -80 °C for ICP-MS analysis.

2.9. Determination of Si and Sn

The total concentration of Si and Sn was determined by ICP-MS, Agilent 7900 (Agilent Technologies). ICP-MS parameters were optimized to obtain the best signal-to-noise ratio for ^{29}Si and ^{119}Sn, while the oxide ratio is lower than 1.5%. The solution of Al and Sb (50 µg/l) was used as internal standards to compensate for a possible matrix effect, and instrumental drift. Set of calibration standards (0-10-100 and 1000 µg/l of Si and 0-1-10 and 100 µg/l of Sn) was used for quantification. Prior to the analysis, the samples were mixed with 1.5 ml of 2% nitric acid and placed into ultrasonic bath to lyse the cells.

2.10. Holographic life cell imaging

To support ICP-MS data, we used holographic life cell imaging of SK-OV-3 cells. The cells were seeded on 35 mm petri-dishes with glass bottom (Ibidi) and exposed to 10 µg/ml of M4 dispersed in dimethyl sulfoxide (Sigma-Aldrich) for 24 hours. After incubation, the cells were scanned using a holographic microscope - the 3D Cell Explorer (Nano Live). Image output was evaluated in STEVE 3D Cell Explorer software counterpart (Nano Live).

Scheme 2. Synthesis of materials **M1**-**M4**
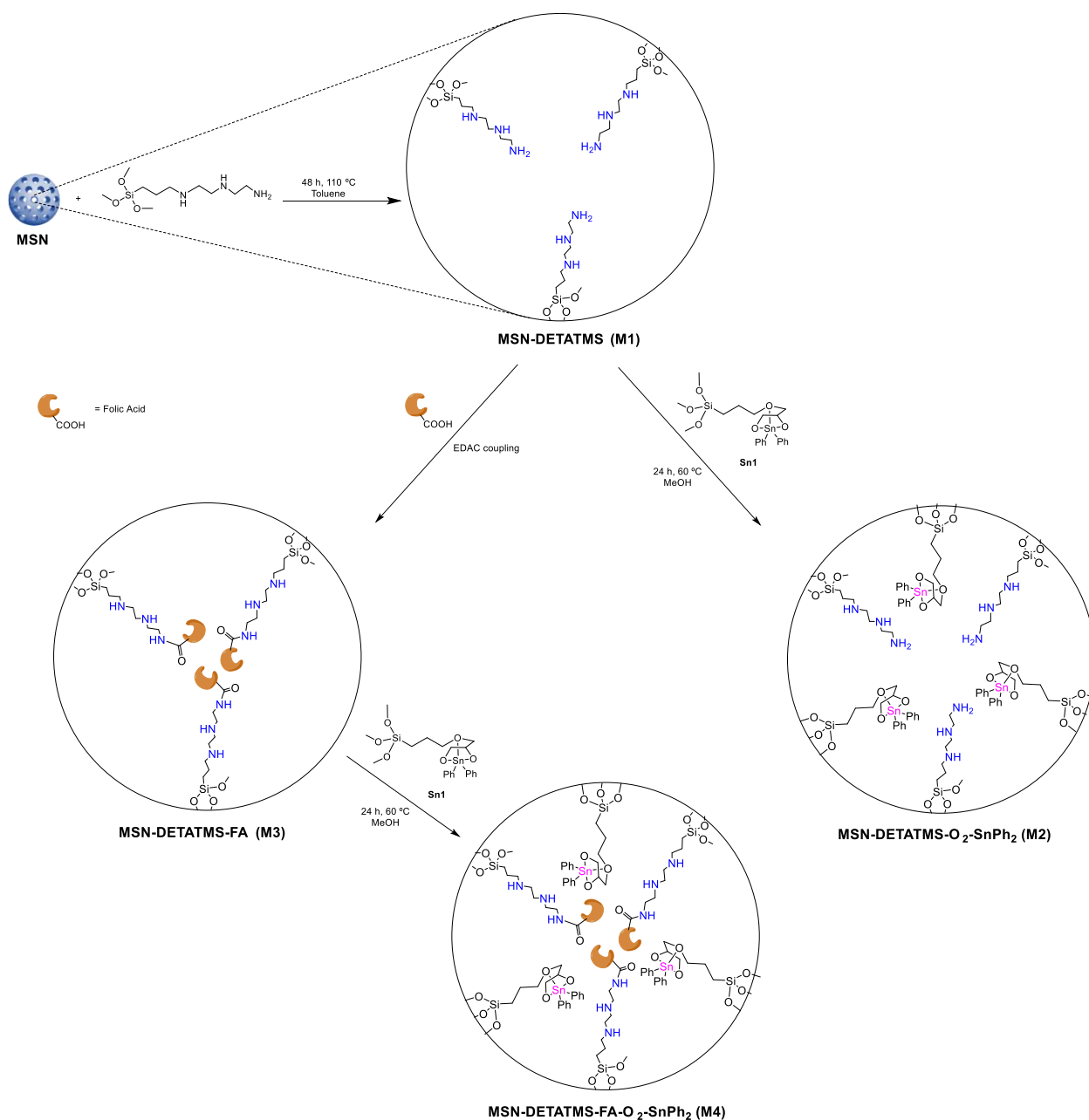
2.11. Cell death analysis

Cell viability was measured using colourimetric MTT assay as described previously[41]. Data were analyzed in GraphPadPrism software and expressed as IC_{50} values (compound concentrations that produce 50% of cell growth inhibition). All experiments were performed in five technical replicates and each experiment in three biologically independent replicates.

Early and late apoptosis was determined by Annexin V-FITC/ propidium iodide (PI) FACS double staining assay. Briefly, cells were trypsinized and washed twice with PBS. Cell pellets were then resuspended in 100 µl of staining solution prepared from 1x binding buffer, FITC-Annexin V (both Biolegend) and PI (Sigma-Aldrich) and incubated for 30 min in the dark at room temperature. The fluorescence signal was detected by flow cytometry (FACS Verse, BD Biosciences). Cells were divided into quadrants separated according to positivity or negativity for FITC (Annexin V) and PE (PI) fluorescence. The percentages of apoptotic cells were quantified using FCS Express 4 software (BD Biosciences).

5-(and-6)-chloromethyl-2′,7′-dichlorodihydrofluorescein diacetate, acetyl ester (CM-H2DCFDA) (Invitrogen) was used for fluorescent quantification of reactive oxygen species (ROS) in living cells. SK-OV-3 cells were grown overnight in 96-well plates, washed twice with prewarmed HBSS (Sigma-Aldrich) and then incubated with 1 µM CM-H2DCFDA at 37 °C in the dark. After 30 min, cells were washed twice in HBSS and treated with 10 µg/ml of M1-M4 for 2 hours. Treatment with H_2O_2 (Penta) at 50 µM was used as a positive control. 10 mM N-Acetyl-L-cysteine (NAC, Sigma-Aldrich) served as a negative control. After incubation, ROS were measured using Infinite® M1000 PRO plate reader (Tecan Trading AG) with excitation and emission wavelengths of 498 and 529 nm, respectively.

2.12. Cellular migration and invasion

In scratch (wound healing) assay the cells were grown to 100% confluence and scratched in serum-free medium to avoid cellular proliferation as described previously [42]. Cells were left to re-populate the scratched area for 24 hours and photographs were taken using a digital camera (Hammamatsu) mounted on an inverted microscope Nikon Ti Eclipse. Wound closure rates were analyzed by TScratch software [43].

Invasion of the cells was determined using a CytoSelect 24-well Cell Invasion Assay kit (Cell Biolabs) according to the manufacturer's protocol. In summary, 0.5×10^6 cells in 300 µl serum-free medium containing testing compound were added to the upper chamber pre-coated with basement membrane matrix solution. Subsequently, 0.5 ml of 10% FBS-containing medium was added to the lower chamber as a chemoattractant. The cells were incubated for 36 hours at 37 °C, and then the non-invading cells were removed with cotton swabs. The cells, which had invaded to the bottom of the membrane were fixed and stained with staining solution. The stained cells were dried and dissolved with the extraction solution. Then the samples were measured by a spectrophotometer (TECAN) at 560 nm.

2.13. Analysis of folate receptors

Cultured cells were detached with accutase (Sigma), washed twice with 3% bovine serum albumin (Sigma) in PBS, and stained with antibody against folate receptor alpha (R&D) at room temperature. Followed by washing and incubation with secondary antibody conjugated with AlexaFluor488 (Abcam), cells were analysed by flow cytometry using a FACSVerse (BD Biosciences). Cells stained only with secondary antibody were used as a negative control to determine the relative expression of folate receptor at cellular membrane. Data analysis was performed with FCSExpress version 4. Cells were first gated based on forward and side scatters (FCS-A vs SSC-A, measuring cell size and granularity, respectively) to exclude debris. Single cells were then selected based on FSC-A vs FCS-H parameters and the doublets were excluded. Histograms of specific antibody stained cells were generated and compared to the respective negative control.

2.14. Statistical analysis

One-way ANOVA (analysis of variance) with post-hoc Tukey HSD calculator was used to determine statistically significant differences between the groups. It was performed using the free online web tool available at https://astatsa.com/OneWay_Anova_with_TukeyHSD/. Tests with $p < 0.05$ were considered as significant.

2.15. Release studies

Tin release of the **M2** material as a model was carried out in a pH 7.4 PBS buffer in duplicate. 10 mL of the buffer was added to 10 mg of the studied materials and the suspensions were incubated at 37 °C in a water bath for 1, 6, 24 and 48 h. Subsequently, the suspension was filtered through a nylon filter (0.2 µm) and the obtained solution was analysed by ICP-AES, with a Varian Vista AX Pro Varian 720-ES instrument in triplicate.

3. Results and discussion
### 3.1. Synthesis and characterization of the materials

Partially dehydrated MSN (treated overnight at 80 °C under vacuum) in a toluene solution with the polyamino ligand N^1-(3-trimethoxysilylpropyl)diethylenetriamine (DETATMS) in a 1:1 weight ratio resulted in the corresponding grafting reaction (Scheme 2) yielding the material MSN-DETATMS (**M1**). **M1** was subsequently treated with the diphenyltin(IV) compound **Sn1** (in a theoretical quantity to obtain a 10% wt Sn/SiO$_2$) [obtained previously from the reaction of (3-glycidyloxypropyl)trimethoxysilane and diphenyltin(IV) dichloride in the presence of two equivalents of sodium hydroxide (Scheme 1)] to give the material MSN-DETATMS-O$_2$-SnPh$_2$ (**M2**).

Material **M1** in an aqueous mixture with folic acid (10% wt. relationship FA/SiO$_2$) in the presence of the coupling agent EDAC gave the material MSN-DETATMS-FA (**M3**) (Scheme 2). **M3** has a folate fragment bound to the polyamino ligand via an amido bond. Finally, this material was further functionalized with the tin compound **Sn1** (in a theoretical quantity to obtain a 10% wt Sn/SiO$_2$) to give the material MSN-DETATMS-FA-O$_2$-SnPh$_2$ (**M4**).

All the synthesized materials were characterized by different methods such as powder XRD, X-ray fluorescence (XRF), solid-state ^{13}C NMR spectroscopy, FT-IR spectroscopy and transmission electronic microscopy (TEM).

3.1.1. *Characterization by powder X-ray diffraction studies*

The starting material MSN and the functionalized materials **M1**, **M2** and **M4** have been characterized by powder XRD (Figure 1 and Table 1). All the materials show a high intensity diffraction peak at ca. 2.1º attributed to the Miller plane (100) which confirms the mesoscopic order of the materials attributed to their hexagonal porous structure. The intensity of this peak decreases after the different functionalization reactions due to the partial blocking of the dispersion points of the porous system caused by the incorporation of the organic or organometallic fragments inside the pores. In addition, the position of the peak does not significantly change after functionalization.
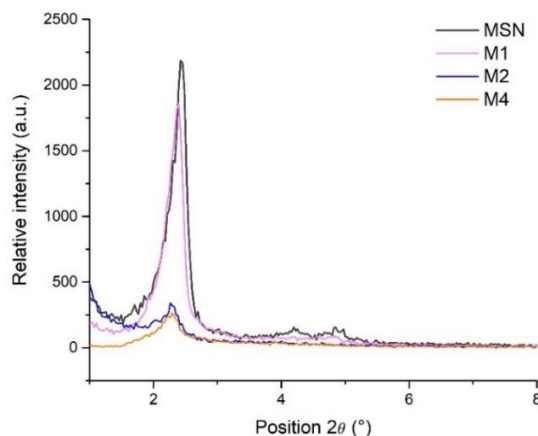
Figure 1. XRD diffraction patterns of MSN, MSN-DETATMS (**M1**), MSN-DETATMS-O$_2$-SnPh$_2$ (**M2**) and MSN-DETATMS-FA-O$_2$-SnPh$_2$ (**M4**).

It is important to note that, the diffractogram of the unmodified material MSN shows, in addition to the peak corresponding to the Miller plane (100), two additional peaks of very low intensity at ca. 3.8 and 4.4° that are assigned to the Miller planes (110) and (200), respectively (Table 1). These peaks of planes (110) and (200) are not visible for **M1**, **M2** and **M4**, due to the dramatic decrease of intensity after the functionalization reactions.

Table 1. Powder XRD data of the materials MSN, **M1**, **M2** and **M4**

Material	*hkl*	2θ (°)	d_{hkl} (nm)	a_0 (nm)
MSN	100	2.4521	3.603	4.160
	110	4.2318	2.088	2.241
	200	4.8973	1.804	2.084
MSN-DETATMS (**M1**)	100	2.3341	3.782	4.367
MSN-DETATMS-O$_2$-SnPh$_2$ (**M2**)	100	2.3102	3.821	4.412
MSN-DETATMS-FA-O$_2$-SnPh$_2$ (**M4**)	100	2.3329	3.784	4.369

3.1.2. Characterization by nitrogen adsorption-desorption isotherms

The starting material MSN and the organotin-functionalized materials **M2** and **M4** (Figure 2) were characterized by nitrogen adsorption-desorption. In the case of the starting material MSN the obtained isotherm is between type IV and type VI [44] as described in the literature for mesoporous silica nanoparticles [23]. In addition, the isotherm of MSN shows a very small hysteresis loop between P/P_0 1.0 and ca. 0.80 due to capillary condensation of nitrogen into the straight pores of the system, in addition, another hysteresis loop was observed between P/P_0 0.4 and 0.15 again attributed to capillary condensation. According to the parameters obtained by this BET isotherm MSN material shows a BET surface of 822 m^2/g and a pore volume of 0.63 cm^3/g and a pore diameter of 3.1 nm (Table 2).
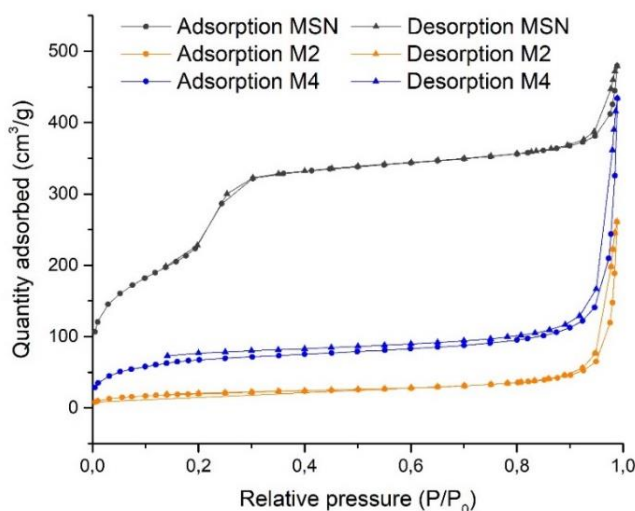
Figure 2. Nitrogen adsorption-desorption isotherms of materials MSN, MSN-DETATMS-O$_2$-SnPh$_2$ (**M2**) and MSN-DETATMS-FA-O$_2$-SnPh$_2$ (**M4**).

After functionalization with the organic and / or organometallic fragments, the nitrogen adsorption-desorption isotherms obtained for **M3** and **M4** were both type III [44] which are indicative of nanoporous or non-porous materials. This indicates that the functionalization with the different ligands or tin compounds of the systems has mainly taken place inside the pores of the mesoporous silica nanoparticles. This results in a dramatic decrease of the BET surface area after functionalization which is more visible in **M4** (functionalized with both FA and the organotin compound) than in **M2** (functionalized only with the polyamino ligand and the organotin compound). The BET surface area of **M2** is 245.5 m^2/g while that of **M4** is only 72.1 m^2/g. From these data one can envisage that the pore occupation by the different supported agents is much higher in **M4** which results in higher congestion of the channels of the nanoparticles leading to an

almost non-porous system after the sequential functionalization. The functionalization inside the pores is confirmed by the dramatic decrease of both the pore volume and pore diameter of **M2** and **M4** when compared with that of the unmodified MSN (Table 2).

Table 2. Textural parameters obtained by nitrogen adsorption-desorption isotherms and quantity of Sn in the material measured by XRF.

Material	S_{BET} (m^2/g)	V_P (cm^3/g)	d_P (nm)	Sn (% wt.)
MSN	822.1	0.64	3.1	-
MSN-DETAMTS-O$_2$SnPh$_2$ (**M2**)	245.5	0.32	<2.0	10.20±0.07
MSN-DETATMS-FA-O$_2$SnPh$_2$ (**M4**)	72.1	0.18	<2.0	9.14±0.04

3.1.3. Characterization by solid-state ^{13}C NMR spectroscopy

Tin-functionalized materials **M2** and **M4** were also characterized by ^{13}C CP MAS spectroscopy (Figure 3). The ^{13}C CP MAS spectra of both systems showed a set of broad signals in the area between 0 and 60 ppm. The appearance of broad signals precludes a precise and non-speculative assignation of each signal to each carbon atom. However, one can easily envisage that the signals correspond to the aliphatic carbon atoms of the polyamino ligand (Si-CH$_2$-CH$_2$-CH$_2$-N and the different N-CH$_2$-CH$_2$-N moieties) and the carbon atoms of the glycydoxypropyl ligand. In addition, in both cases, two signals of medium intensity at *ca.* 130 and 160 ppm were observed and assigned to the carbon atoms of the phenyl rings of the SnPh$_2$ moiety.
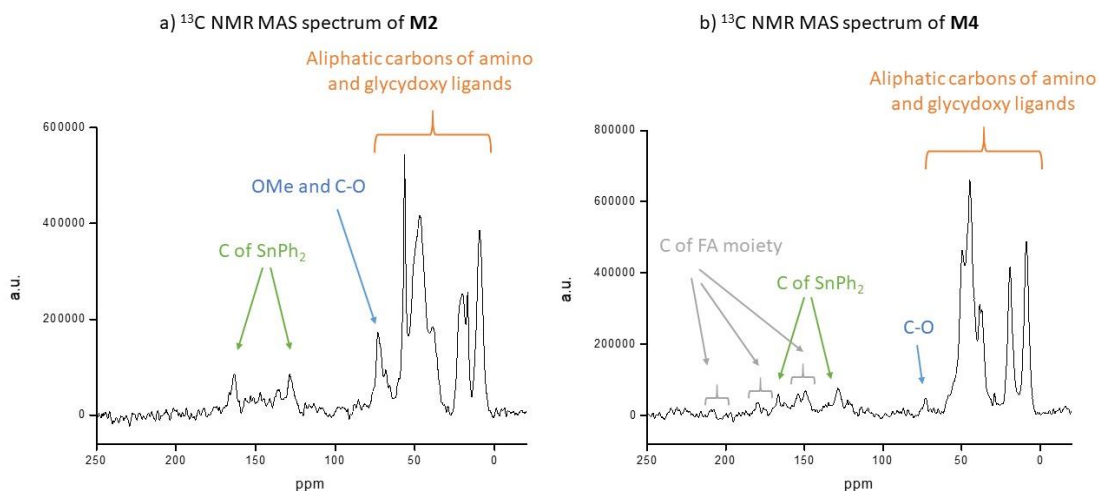
Figure 3. ^{13}C NMR MAS spectra of **M2** and **M4**

In addition, a signal of medium intensity at *ca.* 75 ppm, corresponding to the carbon atoms of the pendant OMe groups coming from the incorporation of the polyamino ligand, was observed in the spectrum of **M2**. Interestingly, in the case of the ^{13}C CP MAS spectrum of material **M4**, the signal at 75 ppm was not observed, as the aqueous reaction mixture used for the incorporation of folic acid did hydrolize the pendant methoxide groups. Nevertheless, the ^{13}C CP MAS spectrum of material **M4** showed some additional signals of low intensity in the area between ca. 145 and 215 ppm, which were attributed to the supported folic acid incorporation, as this fragment has various aromatic carbon atoms and carbonyl carbon atoms of the carboxylic acid or carboxylate and / or of the carboxamide (CONH) groups which usually appear in this area of the spectrum.

3.1.4. Characterization by XRF

For the quantification of tin-functionalization in materials **M2** and **M4**, X-ray fluorescence was carried out in order to determine the % wt. of Sn in the synthesized materials (Table 2). According to the compositional study, material without folic acid (**M2**) presents a slightly higher functionalization of *ca.* 10.20 % wt. Sn compared to that of the nanostructured material containing folic acid (**M4**) which is 9.14 % wt.. This functionalization corresponds to a quantity of 0.859 mmol of Sn complex per gram of material for **M2** and 0.770 mmol of Sn complex per gram of material for **M4**. It is important to note that in **M2** and **M4**, the ratio Si:Sn is of about 6.50 and 5.50, respectively.

3.1.5. Characterization by FT-IR

Tin-functionalized materials **M2** and **M4** have also been characterized by FT-IR spectroscopy (Figure 4 for **M4** and Figure S1 of supplementary material for **M2**). However, as the functionalization rate of the materials with the different ligands is relatively low, and the signals attributed to the silica support are very intense, the study by FT-IR is difficult and a complete analysis of each of the bands of the supported ligands or compounds was precluded due to overlap of some characteristic bands of the ligands or the supported tin complex, with the most intense bands of the silica support.

In this context, when one analyzes the FTIR spectra of tin-functionalized materials **M2** and **M4**, one can see, in both cases, the typical O–H stretching bands attributed to the silanol groups and the adsorbed water molecules (between 3500 and 3200 cm^{-1}). In addition, both spectra present a broad band corresponding to the siloxane (Si–O–Si) group at *ca.* 1100 cm^{-1} and the stretching band of the Si–O bonds, which appears at *ca.* 900 cm^{-1}. Furthermore, the spectra show, at *ca.* 1625 cm^{-1}, the band corresponding to the deformation vibrations of water molecules adsorbed on the surface of the material. In addition, to the signals of the mesoporous silica nanoparticles support, some bands of relatively low intensity are visible in the spectra. In both cases, typical bands of the different supported ligands were observed, thus, C-H and N-H vibration bands were recorded between 2700 and 3400 cm^{-1}, C=C and COO or CON signals were observed between *ca.* 1350 and 1750 cm^{-1}.
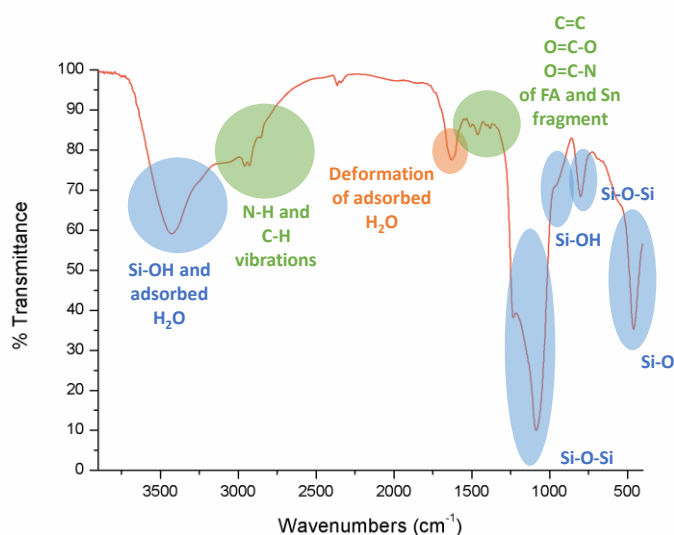

Figure 4. IR spectrum of **M4**

3.1.6. Characterization by TEM

The unmodified MSN and the tin-functionalized mesoporous silica nanoparticles **M2** and **M4** were functionalized by conventional transmission electron microscopy (TEM) in order to determine the particle size and morphology before and after the functionalization processes. The TEM image of the unmodified MSN (Figure 5a) shows that the material is composed of porous

spheres with hexagonal ordered porous parallel channels. When one analyzes the particle size of the nanospheres (by using ImageJ® program, NIH USA) the results show that the nanoparticles have a diameter of ca. 91±9 nm.
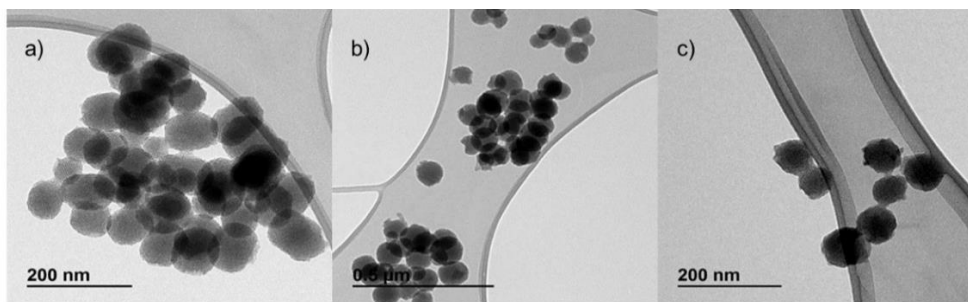

Figure 5. TEM images of a) MSN, b) **M2** and c) **M4**

The TEM images of materials **M2** (Figure 5b) and **M4** (Figure 5c) show that the spherical morphology is retained after functionalization and that there is no significant change in the particle size which is 97±7 nm and 91±12 nm for **M2** and **M4**, respectively.

3.1.7. Characterization by electrochemical techniques

Differential pulse voltammograms of the tin-functionalized materials **M2** and **M4** have been studied. The voltammetric response showed signals due to the tin species attached to the silica nanostructured materials. Figure 6 presents the DPV observed for **M2** and **M4** after immersion of the graphite/silica working electrode in aqueous electrolyte solutions at pH 7.4 (physiological) and 5.5 (endosomic) buffers. In all cases, a cathodic peak at around -1.00 V, assigned to the Sn(IV)/Sn(II) couple, was observed, confirming the tethering of the tin-containing moiety to the mesoporous silica nanoparticles. When one compares the reduction peak, in both cases (materials **M2** and **M4**), the reduction only slightly changes at different pH conditions indicating a very low influence of the medium in the reduction ability of the tin atom.
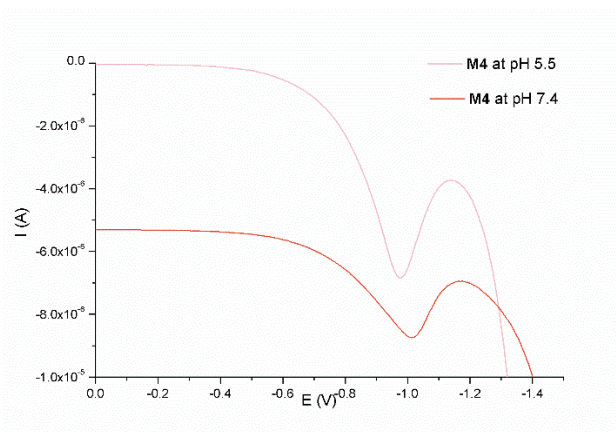

Figure 6. Differential pulse voltammograms (75 mV modulation amplitude) of **M4** / graphite electrode immediately after immersion in aqueous phosphate buffer pH 7.4 and pH 5.5 vs Ag/AgCl/KCl (3 M) as reference electrode

3.2. Biological studies of the synthesized mesoporous silica nanoparticles
3.2.1. Cellular uptake

For targeted delivery to the tumour, the cellular target usually possesses a membrane associated antigen. Folate receptor (FR) is a valuable therapeutic target that is highly expressed in a variety of cancers [45]. Two general strategies have been developed for the targeted delivery of drugs to FR-positive tumour cells: by coupling to a monoclonal antibody against the receptor

and by coupling to a high affinity ligand [46]. In our work, we used the second strategy based on FA-conjugates. Two different human cancer cell lines A549, SK-OV-3 and non-cancerous human embryonic kidney cell line HEK 293 were exposed to **M1**-**M4** in order to determine their accumulation inside the cells. Importantly, **M3** and **M4**, bearing folate moiety, showed significantly higher intracellular accumulation in all three cell lines in comparison with cells exposed to **M1** or **M2** (Figure 7 A-C).
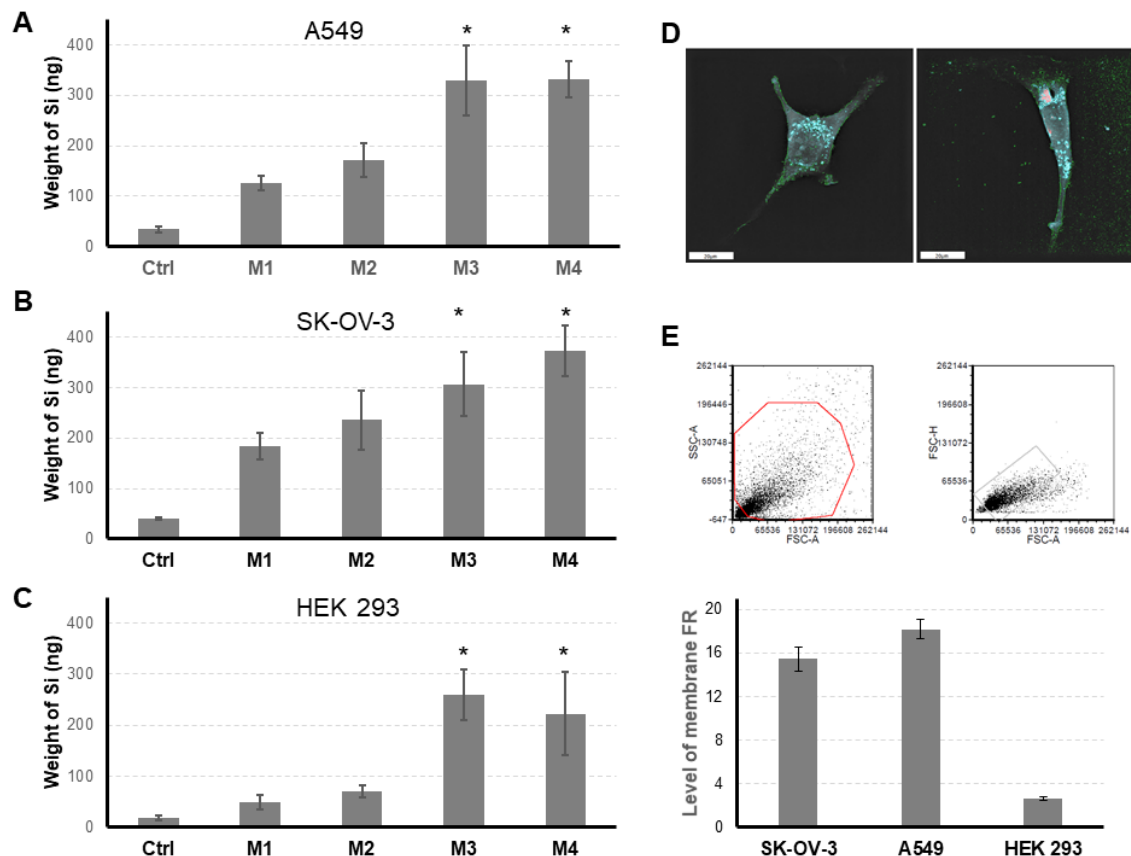
Figure 7. Intracellular accumulation of MSN determined by ICP-MS. Amount of silicon (Si) was calculated in relation to 2.2×10^6 of cells. Three independent biological experiments were performed to construct the graphs for (A) A549 cells and two for (B) SK-OV-3 and (C) HEK 293 cells, *$P<0.05$ vs. **M1**. (D) Holographic life cell imaging of untreated SK-OV-3 cells (left) and 24 hours after treatment with **M4** (right). The green colour shows the outer membrane of the cell. Blue colour highlights the internal membrane structure with bright blue lipid vesicles. Distribution of the **M4** substance is displayed in red. (E) Flow cytometry plots showing the gating strategy to determine viable (left upper part) and individual (right upper part) cellular population. Graph (lower part) shows the level of membrane FR in individual cell lines.

Holographic life cell imaging of ovarian cancer cells SK-OV-3 confirmed intracellular, most probably cytoplasmic, accumulation of **M4** (Figure 7D).Taken together, this data confirms that folate fragment functionalization of nanostructured materials serving as a vector for metallodrugs significantly enhances their cellular uptake. Accordingly, flow cytometry analysis of FRs revealed very similar and relatively high level of FRs in membranes of A549 and SK-OV-3 cells, compared to HEK 293 cells which show markedly lower level of FRs (Figure 7E). These findings correspond with more efficient accumulation of **M3** and **M4**, thus highlighting the positive impact of the presence of folate receptors on cellular uptake of mesoporous silica nanoparticles functionalized with the folate moiety.

In parallel, cellular uptake of tin (Sn) was determined. As expected, tin was detected in cells treated with **M2** or **M4**, the latter having a much higher quantity. However, the ratio Sn:Si is similar for **M2** and **M4** (Table 3).

Table 3. Cytotoxicity and cellular uptake of **M1**-**M4**

Materials	A549			SK-OV-3			HEK 293		
	IC_{50} µg/mL	Si (ng)*	Sn (ng)#	IC_{50} µg/mL	Si (ng)	Sn (ng)	IC_{50} µg/mL	Si (ng)	Sn (ng)
M1	94.2±19.1	125±15	ND†	>200	183±27	ND†	80.8±13.3	49±13	ND†
M2	29.6±18.3 [3.0±1.9]§	195±33	19.9±6.5	16.3±8.9 [1.7±0.9]§	236±59	31.2±10.9	40.4±9.8 [4.1±1.0]§	71±12	11.7±6.6
M3	42.2±12.5	328±70	ND	22.4±9.3	307±63	ND	39.4±8.7	260±49	ND
M4	5.7±1.6 [0.5±0.1]§	331±36	41.8±9.3	9.6±7.5 [0.9±0.7]§	374±50	77.2±28.9	39.5±8.8 [3.6±0.8]§	223±81	40.0±10.3

* Intracellular accumulation of Si per $2.2{\times}10^6$ cells
\# Intracellular accumulation of Sn per $2.2{\times}10^6$ cells
† Not detected
§ data in brackets correspond to Sn quantity

Additionally, model release studies were carried out for **M2** in PBS at different times to observe if tin-containing soluble species were release in the medium after 48 hours at 37 ºC (See Figure S2 and Table S1 of Supplementary Material). The results confirm that these nanomaterials again seem to work as "non-classical" drug-delivery nanosystems as they do not release to the medium the Sn-containing metal-based drug as only less than 1% of the loaded tin is released to the physiologic medium. Therefore, again in this case, **M2** and **M4** act as entire nanoparticulated therapeutic systems without the need of the delivery of tin-soluble active species.

3.2.2. Cell death determination

The rate of intracellular accumulation of nanoparticles in selected cell lines clearly reflects their cytotoxic effect determined by MTT assay especially for **M4** bearing both FA and organotin complex (Table 3). To confirm the selectivity of prepared MSN, extended panel of various cancer cell lines was subjected to MTT assay. Importantly, cytotoxicity testing revealed a similar trend for all tested cancer cell lines (Table S2 of Supplementary Material). Briefly, **M1** nanoparticles showed the lowest toxicity. The addition of the organotin complex enhanced the cytotoxic effects of **M2** and functionalization of MSN with both FA and the organotin moiety resulted in a clear increase in cytotoxicity of **M4** towards all cancer cell lines (Table S2 of Supplementary Material).

The investigation of cell death mechanism associated with cytotoxic effects of MSN confirmed the induction of apoptosis predominantly after exposure to **M4** in both A549 and SK-OV-3 cells (Figure 8). Interestingly, in SK-OV-3 cells with an intrinsic resistance to cisplatin [47], faster apoptosis progress was observed in response to **M4**, as documented by a significantly larger proportion of late apoptotic cells versus early apoptotic cells in comparison with cisplatin treated cells. Organotin compounds were also shown to induce production of reactive oxygen species (ROS), which may result in significant damage to cell structures.
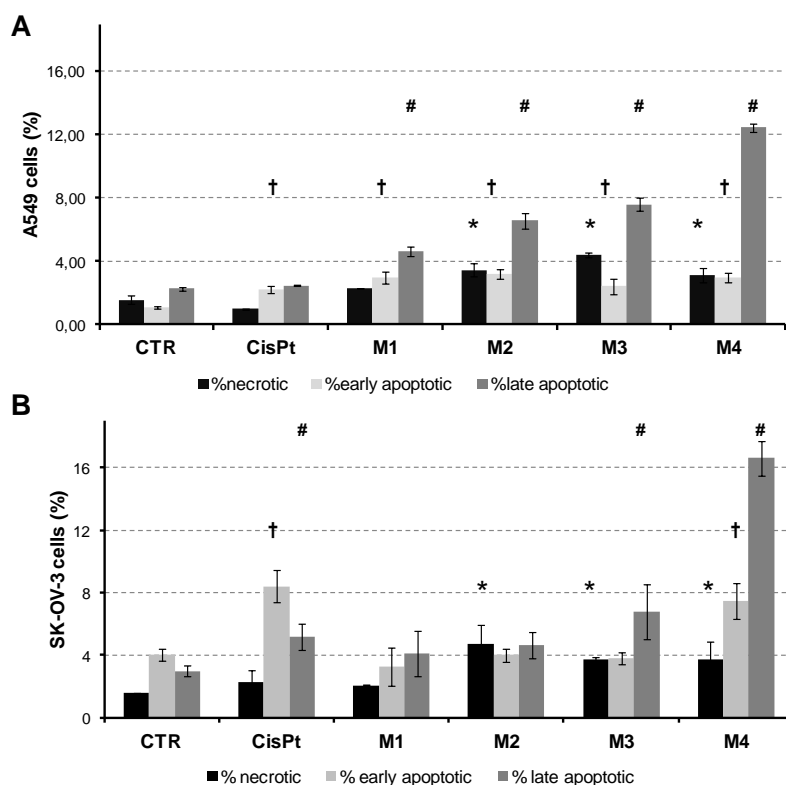
Figure 8. The induction of apoptosis was analyzed by Annexin V-FITC/PI FACS double staining assay for (A) A549 and (B) SK-OV-3 cells. *necrotic, †early apoptotic and #late apoptotic cells exposed to MSN as indicated showing significant changes ($p<0.05$) in comparison with untreated (CTR) cells. Treatment with 10 µM cisplatin served as a positive control of apoptosis induction.

Thus **M4** as the most potent inducer of apoptosis was selected to analyze its effect on ROS production. Indeed, elevated ROS levels were detected in both A549 and SK-OV-3 cells (Figure 9). On the other hand, subsequent testing of **M1**, **M2** and **M4** nanoparticles showed only insignificant changes in ROS production for both cell lines (data not shown).
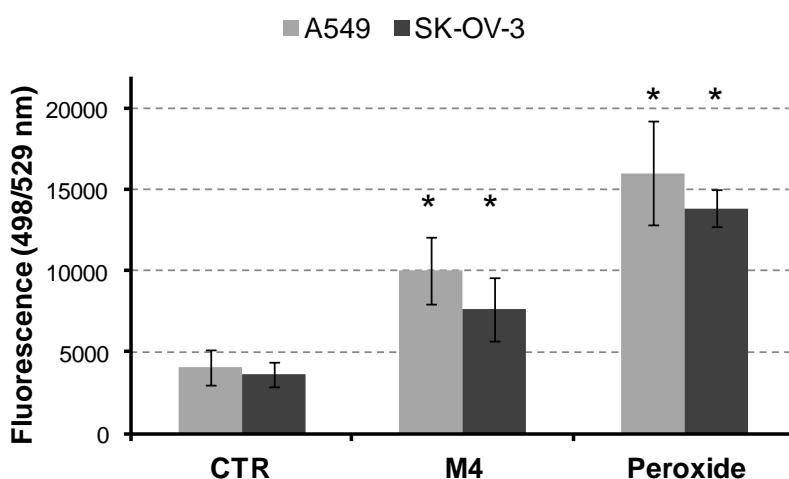

Figure 9. ROS production in untretaed cells (CTR), cells treated with **M4** and peroxide, *P<0.05 compared to CTR.

3.2.3. Evaluation of migrastatic activity

Metastasis is a major health threat for most cancer patients, thus anti-metastatic drugs that reduce cell migration and invasion are critical for cancer treatment [48]. Very recently, a new term "migrastatic species" was introduced, which characterizes a class of drugs that influence all modes of cancer cell invasion and metastasis and distinguishes this kind of systems from common antiproliferative drugs [49]. Migrastatic activity of MSN was first analyzed by wound healing assay in A549 (Figure 10A, Figure S3 of Supplementary Material) and SK-OV-3 cells (Figure S3 of Supplementary Material). Interestingly, the inhibition of migration was observed only for A549 cells in response to all types of nanoparticles except **M1**. However, **M4** blocked cell migration to the largest extent. MDA-MB-231, a highly aggressive, invasive and poorly differentiated breast cancer cell line, was then selected to confirm anti-migratory activity of MSN (Figure 10B). Indeed, clear inhibition of cell migration was observed after exposure of MDA-MB-231 cells to MSN, predominantly **M4** showing the greatest ability to block cellular motility compared to other MSN.

In general, cancer metastasis involves the invasion of a tumour cell to a blood or lymph vessel, intravasation into the vessel, extravasation from the blood vessel in another location, and invasion into the tissue to form a secondary tumour. Cell invasion is a complex process, which can be defined as the migration of cells within a tissue in response to various signals [50]. Thus, we also tested the effect of MSN on cell invasiveness. Interestingly, **M4** significantly inhibited invasiveness of both A549 and SK-OV-3 cells, as well as MDA-MB-231 cells (Figure 11, Figure S4 of Supplementary Material).
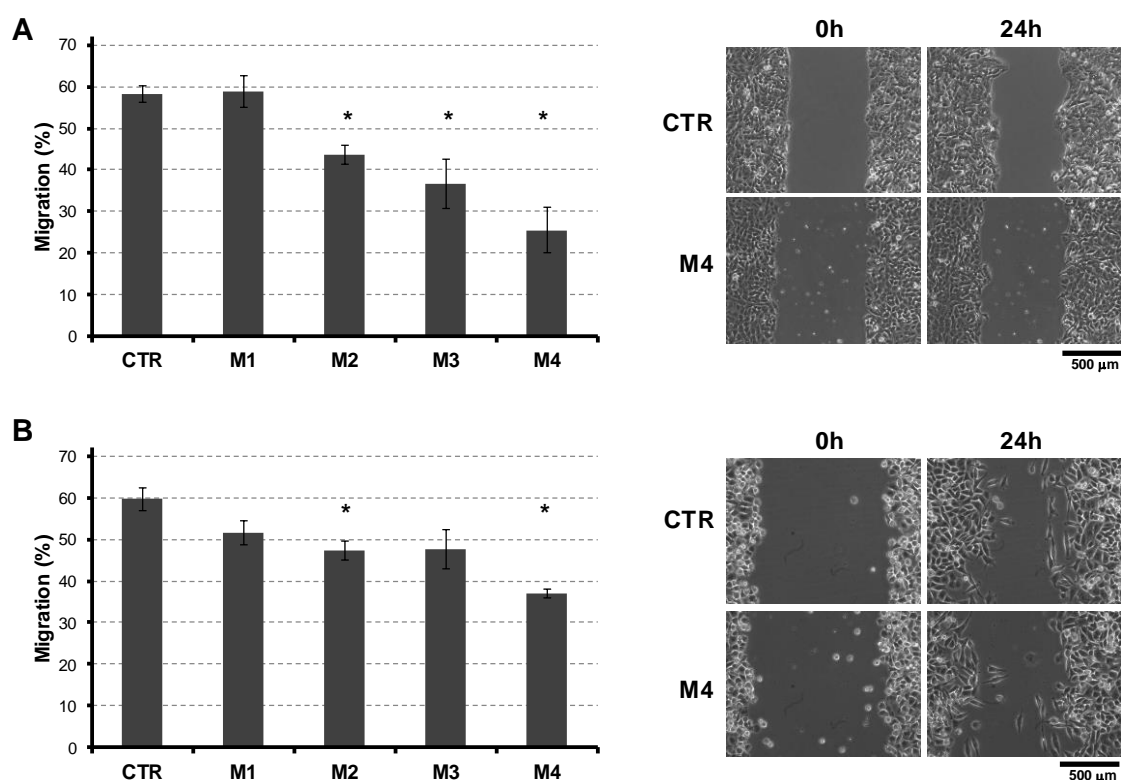
Figure 10. Wound healing assay for (A) A549 cells and (B) MDA-MB-231 cells with materials **M1**-**M4**, *P<0.05 compared to CTR.
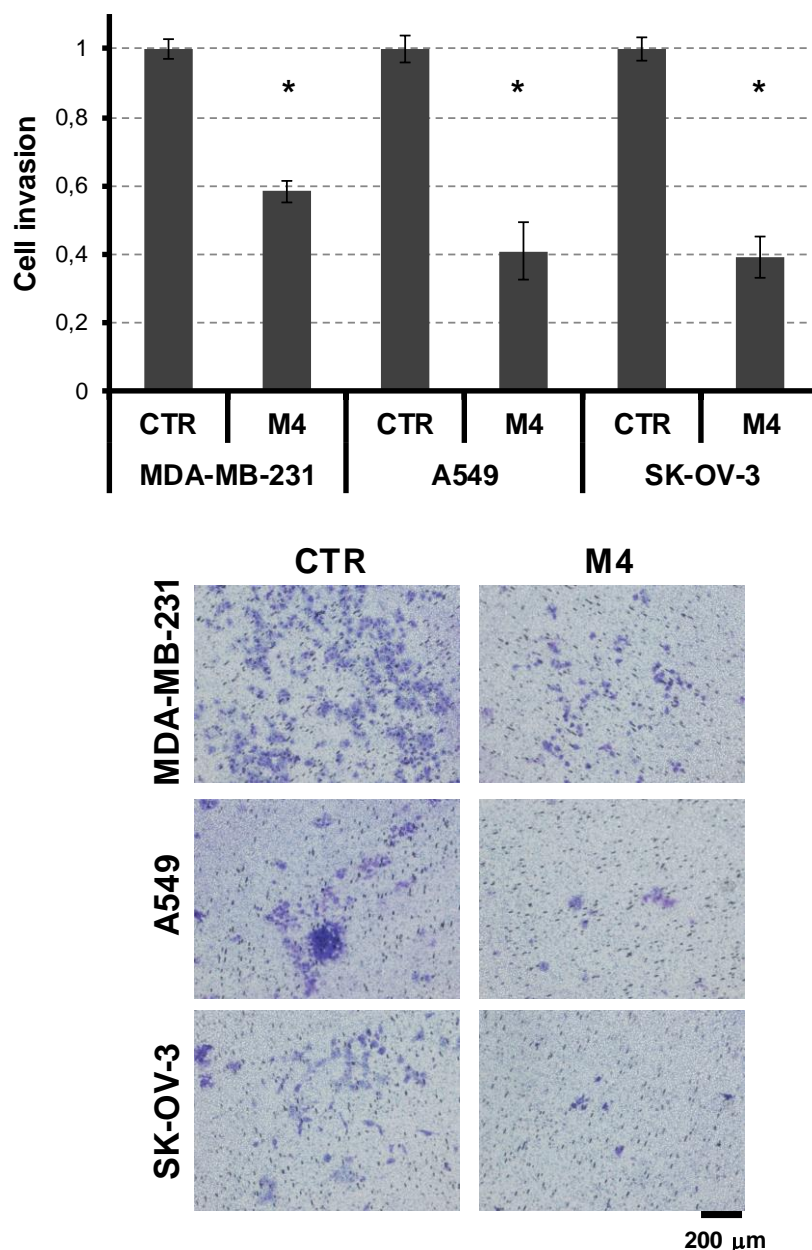
Figure 11. Invasion assay of MDA-MB-231 (M231), A549 and SK-OV-3 cells with the material **M4**, *P<0.05 compared to CTR.

4. Conclusions

We have synthesized and characterized different tin-functionalized mesoporous silica nanoparticles with and without a folate fragment in their structure. All the synthesized nanomaterials have been tested *in vitro* against different cancer and non-cancer cells, in order to determine several aspects of their cytotoxic mechanism. The results show that cell uptake is much higher for those materials with the folic acid fragment in cells which overexpress folate receptors such as MDA-MB-231 and A549, indicating that the folate strategy for improving cell internalization is adequate for enhancing the potential cytotoxic nature of the materials. In addition, the cytotoxic studies revealed a clear relationship between the cytotoxicity and accumulation of nanoparticles inside the cells. In addition, cytotoxic effects confirmed the induction of apoptosis, predominantly after exposure to **M4**, in A549 and SK-OV-3 cells with an intrinsic resistance to cisplatin. Faster apoptosis progress was observed in response to **M4**, which

17

indicates a promising potential anticancer application of this tin-containing material. In addition, elevated ROS levels were detected in both A549 and SK-OV-3 cells when treated with **M4** nanoparticles. Cell migration and cell invasion were tested and the results showed that these processes were significantly decreased when using materials with the cytotoxic tin-containing moieties. In conclusion, this study has shown the potential applicability of tin-containing mesoporous silica nanoparticles functionalized with folate fragments (**M4**) in future chemotherapeutic actions.

Acknowledgements

References

[1] Worldwide cancer statistics, Cancer Research UK. (2019). https://www.cancerresearchuk.org/health-professional/cancer-statistics/worldwide-cancer (accessed May 5, 2019).

[2] Cancer tomorrow, (2019). http://gco.iarc.fr/tomorrow/home (accessed May 5, 2019).

[3] B. Rosenberg, L. VanCamp, The successful regression of large solid sarcoma 180 tumors by platinum compounds, Cancer Res. 30 (1970) 1799–1802.

[4] U. Ndagi, N. Mhlongo, M.E. Soliman, Metal complexes in cancer therapy - an update from drug design perspective, Drug Des Devel Ther. 11 (2017) 599–616. https://doi.org/10.2147/DDDT.S119488.

[5] K.D. Mjos, C. Orvig, Metallodrugs in medicinal inorganic chemistry, Chem. Rev. 114 (2014) 4540–4563. https://doi.org/10.1021/cr400460s.

[6] W.A. Wani, S. Prashar, S. Shreaz, S. Gómez-Ruiz, Nanostructured materials functionalized with metal complexes: In search of alternatives for administering anticancer metallodrugs, Coordination Chemistry Reviews. 312 (2016) 67–98. https://doi.org/10.1016/j.ccr.2016.01.001.

[7] M. Poursharifi, M.T. Wlodarczyk, A.J. Mieszawska, Nano-Based Systems and Biomacromolecules as Carriers for Metallodrugs in Anticancer Therapy, Inorganics. 7 (2019) 2. https://doi.org/10.3390/inorganics7010002.

[8] D. Pérez-Quintanilla, S. Gómez-Ruiz, Ž. Žižak, I. Sierra, S. Prashar, I. del Hierro, M. Fajardo, Z.D. Juranić, G.N. Kaluđerović, A New Generation of Anticancer Drugs: Mesoporous Materials Modified with Titanocene Complexes, Chemistry – A European Journal. 15 (2009) 5588–5597. https://doi.org/10.1002/chem.200900151.

[9] Y. Ellahioui, S. Prashar, S. Gómez-Ruiz, A Short Overview on the Biomedical Applications of Silica, Alumina and Calcium Phosphate-based Nanostructured Materials, Curr. Med. Chem. 23 (2016) 4450–4467.

[10] G.N. Kaluderović, D. Pérez-Quintanilla, Z. Zizak, Z.D. Juranić, S. Gómez-Ruiz, Improvement of cytotoxicity of titanocene-functionalized mesoporous materials by the increase of the titanium content, Dalton Trans. 39 (2010) 2597–2608. https://doi.org/10.1039/b920051g.

[11] G.N. Kaluđerović, D. Pérez-Quintanilla, I. Sierra, S. Prashar, I. del Hierro, Ž. Žižak, Z.D. Juranić, M. Fajardo, S. Gómez-Ruiz, Study of the influence of the metal complex on the cytotoxic activity of titanocene-functionalized mesoporous materials, J. Mater. Chem. 20 (2010) 806–814. https://doi.org/10.1039/B919269G.

[12] A. García-Peñas, S. Gómez-Ruiz, D. Pérez-Quintanilla, R. Paschke, I. Sierra, S. Prashar, I. del Hierro, G.N. Kaluđerović, Study of the cytotoxicity and particle action in human cancer cells of titanocene-functionalized materials with potential application against tumors, J. Inorg. Biochem. 106 (2012) 100–110. https://doi.org/10.1016/j.jinorgbio.2011.09.033.

[13] M.Z. Bulatović, D. Maksimović-Ivanić, C. Bensing, S. Gómez-Ruiz, D. Steinborn, H. Schmidt, M. Mojić, A. Korać, I. Golić, D. Pérez-Quintanilla, M. Momčilović, S. Mijatović, G.N. Kaluđerović, Organotin(IV)-loaded mesoporous silica as a biocompatible strategy in cancer

treatment, Angew. Chem. Int. Ed. Engl. 53 (2014) 5982–5987. https://doi.org/10.1002/anie.201400763.

[14] J. Ceballos-Torres, P. Virag, M. Cenariu, S. Prashar, M. Fajardo, E. Fischer-Fodor, S. Gómez-Ruiz, Anti-cancer Applications of Titanocene-Functionalised Nanostructured Systems: An Insight into Cell Death Mechanisms, Chemistry – A European Journal. 20 (2014) 10811–10828. https://doi.org/10.1002/chem.201400300.

[15] J. Ceballos-Torres, S. Prashar, M. Fajardo, A. Chicca, J. Gertsch, A.B. Pinar, S. Gómez-Ruiz, Ether-Substituted Group 4 Metallocene Complexes: Cytostatic Effects and Applications in Ethylene Polymerization, Organometallics. 34 (2015) 2522–2532. https://doi.org/10.1021/om5012209.

[16] C. Bensing, M. Mojić, S. Gómez-Ruiz, S. Carralero, B. Dojčinović, D. Maksimović-Ivanić, S. Mijatović, G.N. Kaluđerović, Evaluation of functionalized mesoporous silica SBA-15 as a carrier system for Ph3Sn(CH2)3OH against the A2780 ovarian carcinoma cell line, Dalton Trans. 45 (2016) 18984–18993. https://doi.org/10.1039/c6dt03519a.

[17] S. Gómez-Ruiz, A. García-Peñas, S. Prashar, A. Rodríguez-Diéguez, E. Fischer-Fodor, Anticancer Applications of Nanostructured Silica-Based Materials Functionalized with Titanocene Derivatives: Induction of Cell Death Mechanism through TNFR1 Modulation, Materials (Basel). 11 (2018) 224. https://doi.org/10.3390/ma11020224.

[18] D. Díaz-García, D. Cenariu, Y. Pérez, P. Cruz, I. del Hierro, S. Prashar, E. Fischer-Fodor, S. Gómez-Ruiz, Modulation of the mechanism of apoptosis in cancer cell lines by treatment with silica-based nanostructured materials functionalized with different metallodrugs, Dalton Trans. 47 (2018) 12284–12299. https://doi.org/10.1039/C8DT01677A.

[19] I. del Hierro, S. Gómez-Ruiz, Y. Pérez, P. Cruz, S. Prashar, M. Fajardo, Mesoporous SBA-15 modified with titanocene complexes and ionic liquids: interactions with DNA and other molecules of biological interest studied by solid state electrochemical techniques, Dalton Trans. 47 (2018) 12914–12932. https://doi.org/10.1039/C8DT02011F.

[20] Y. Ellahioui, M. Patra, C. Mari, R. Kaabi, J. Karges, G. Gasser, S. Gómez-Ruiz, Mesoporous silica nanoparticles functionalised with a photoactive ruthenium(II) complex: exploring the formulation of a metal-based photodynamic therapy photosensitiser, Dalton Trans. 48 (2019) 5940–5951. https://doi.org/10.1039/C8DT02392A.

[21] D. Maksimović-Ivanić, M. Bulatović, D. Edeler, C. Bensing, I. Golić, A. Korać, G.N. Kaluđerović, S. Mijatović, The interaction between SBA-15 derivative loaded with Ph3Sn(CH2)6OH and human melanoma A375 cell line: uptake and stem phenotype loss, J Biol Inorg Chem. 24 (2019) 223–234. https://doi.org/10.1007/s00775-019-01640-x.

[22] D. Edeler, D. Drača, V. Petković, F. Natalio, D. Maksimović-Ivanić, S. Mijatović, H. Schmidt, G.N. Kaluđerović, Impact of the mesoporous silica SBA-15 functionalization on the mode of action of Ph3Sn(CH2)6OH, Materials Science and Engineering: C. 100 (2019) 315–322. https://doi.org/10.1016/j.msec.2019.03.010.

[23] D. Díaz-García, P.R. Ardiles, S. Prashar, A. Rodríguez-Diéguez, P.L. Páez, S. Gómez-Ruiz, Preparation and Study of the Antibacterial Applications and Oxidative Stress Induction of Copper Maleamate-Functionalized Mesoporous Silica Nanoparticles, Pharmaceutics. 11 (2019) 30. https://doi.org/10.3390/pharmaceutics11010030.

[24] V.S. Bollu, A.K. Barui, S.K. Mondal, S. Prashar, M. Fajardo, D. Briones, A. Rodríguez-Diéguez, C.R. Patra, S. Gómez-Ruiz, Curcumin-loaded silica-based mesoporous materials: Synthesis, characterization and cytotoxic properties against cancer cells, Mater Sci Eng C Mater Biol Appl. 63 (2016) 393–410. https://doi.org/10.1016/j.msec.2016.03.011.

[25] R. Kotcherlakota, A.K. Barui, S. Prashar, M. Fajardo, D. Briones, A. Rodríguez-Diéguez, C.R. Patra, S. Gómez-Ruiz, Curcumin loaded mesoporous silica: an effective drug delivery system for cancer treatment, Biomater. Sci. 4 (2016) 448–459. https://doi.org/10.1039/C5BM00552C.

[26] M. Fernández, F. Javaid, V. Chudasama, Advances in targeting the folate receptor in the treatment/imaging of cancers, Chem. Sci. 9 (2018) 790–810. https://doi.org/10.1039/C7SC04004K.

[27] J. de Oliveira Silva, R.S. Fernandes, C.M. Ramos Oda, T.H. Ferreira, A.F. Machado Botelho, M. Martins Melo, M.C. de Miranda, D. Assis Gomes, G. Dantas Cassali, D.M. Townsend, D. Rubello, M.C. Oliveira, A.L.B. de Barros, Folate-coated, long-circulating and pH-sensitive liposomes enhance doxorubicin antitumor effect in a breast cancer animal model, Biomedicine & Pharmacotherapy. 118 (2019) 109323. https://doi.org/10.1016/j.biopha.2019.109323.

[28] Y.I. Poltavets, A.S. Zhirnik, V.V. Zavarzina, Y.P. Semochkina, V.G. Shuvatova, A.A. Krasheninnikova, S.V. Aleshin, D.O. Dronov, E.A. Vorontsov, V.Yu. Balabanyan, G.A. Posypanova, In vitro anticancer activity of folate-modified docetaxel-loaded PLGA nanoparticles against drug-sensitive and multidrug-resistant cancer cells, Cancer Nanotechnology. 10 (2019). https://doi.org/10.1186/s12645-019-0048-x.

[29] Y. Liu, Y. Zong, Z. Yang, M. Luo, G. Li, W. Yingsa, Y. Cao, M. Xiao, T. Kong, J. He, X. Liu, J. Lei, Dual-Targeted Controlled Delivery Based on Folic Acid Modified Pectin-Based Nanoparticles for Combination Therapy of Liver Cancer, ACS Sustainable Chem. Eng. 7 (2019) 3614–3623. https://doi.org/10.1021/acssuschemeng.8b06586.

[30] S. Shen, Y. Li, Y. Xiao, Z. Zhao, C. Zhang, J. Wang, H. Li, F. Liu, N. He, Y. Yuan, Y. Lu, S. Guo, Y. Wang, W. Liao, Y. Liao, Y. Chen, J. Bin, Folate-conjugated nanobubbles selectively target and kill cancer cells via ultrasound-triggered intracellular explosion, Biomaterials. 181 (2018) 293–306. https://doi.org/10.1016/j.biomaterials.2018.07.030.

[31] W. Qu, B. Meng, Y. Yu, S. Wang, Folic acid-conjugated mesoporous silica nanoparticles for enhanced therapeutic efficacy of topotecan in retina cancers, International Journal of Nanomedicine. (2018). https://doi.org/10.2147/IJN.S142668.

[32] A.M. Khattabi, W.H. Talib, D.A. Alqdeimat, A targeted drug delivery system of anti-cancer agents based on folic acid-cyclodextrin-long polymer functionalized silica nanoparticles, Journal of Drug Delivery Science and Technology. 41 (2017) 367–374. https://doi.org/10.1016/j.jddst.2017.07.025.

[33] Q. Liu, N. Xu, L. Liu, J. Li, Y. Zhang, C. Shen, K. Shezad, L. Zhang, J. Zhu, J. Tao, Dacarbazine-Loaded Hollow Mesoporous Silica Nanoparticles Grafted with Folic Acid for Enhancing Antimetastatic Melanoma Response, ACS Appl. Mater. Interfaces. 9 (2017) 21673–21687. https://doi.org/10.1021/acsami.7b05278.

[34] P. Khosravian, M.S. Ardestani, M. Khoobi, S.N. Ostad, F.A. Dorkoosh, H.A. Javar, M. Amanlou, Mesoporous silica nanoparticles functionalized with folic acid/methionine for active targeted delivery of docetaxel, OncoTargets and Therapy. (2016). https://doi.org/10.2147/OTT.S113815.

[35] N.Ž. Knežević, J. Mrđanović, I. Borišev, S. Milenković, Đ. Janaćković, F. Cunin, A. Djordjevic, Hydroxylated fullerene-capped, vinblastine-loaded folic acid-functionalized mesoporous silica nanoparticles for targeted anticancer therapy, RSC Adv. 6 (2016) 7061–7065. https://doi.org/10.1039/C5RA22937E.

[36] J. Lu, Z. Li, J.I. Zink, F. Tamanoi, In vivo tumor suppression efficacy of mesoporous silica nanoparticles-based drug-delivery system: enhanced efficacy by folate modification, Nanomedicine: Nanotechnology, Biology and Medicine. 8 (2012) 212–220. https://doi.org/10.1016/j.nano.2011.06.002.

[37] J. Fan, G. Fang, X. Wang, F. Zeng, Y. Xiang, S. Wu, Targeted anticancer prodrug with mesoporous silica nanoparticles as vehicles, Nanotechnology. 22 (2011) 455102. https://doi.org/10.1088/0957-4484/22/45/455102.

[38] J. Wang, Y. Wang, Q. Liu, L. Yang, R. Zhu, C. Yu, S. Wang, Rational Design of Multifunctional Dendritic Mesoporous Silica Nanoparticles to Load Curcumin and Enhance Efficacy for Breast Cancer Therapy, ACS Appl. Mater. Interfaces. 8 (2016) 26511–26523. https://doi.org/10.1021/acsami.6b08400.

[39] S. Malekmohammadi, H. Hadadzadeh, Z. Amirghofran, Preparation of folic acid-conjugated dendritic mesoporous silica nanoparticles for pH-controlled release and targeted delivery of a cyclometallated gold(III) complex as an antitumor agent, Journal of Molecular Liquids. 265 (2018) 797–806. https://doi.org/10.1016/j.molliq.2018.07.024.

[40] Y. Zhao, B.G. Trewyn, I.I. Slowing, V.S.-Y. Lin, Mesoporous Silica Nanoparticle-Based Double Drug Delivery System for Glucose-Responsive Controlled Release of Insulin and Cyclic AMP, J. Am. Chem. Soc. 131 (2009) 8398–8400. https://doi.org/10.1021/ja901831u.

[41] T. Hodík, M. Lamač, L. Červenková Šťastná, J. Karban, L. Koubková, R. Hrstka, I. Císařová, J. Pinkas, Titanocene Dihalides and Ferrocenes Bearing a Pendant α-d-Xylofuranos-5-yl or α-d-Ribofuranos-5-yl Moiety. Synthesis, Characterization, and Cytotoxic Activity, Organometallics. 33 (2014) 2059–2070. https://doi.org/10.1021/om500200r.

[42] J.E.N. Jonkman, J.A. Cathcart, F. Xu, M.E. Bartolini, J.E. Amon, K.M. Stevens, P. Colarusso, An introduction to the wound healing assay using live-cell microscopy, Cell Adhesion & Migration. 8 (2014) 440–451. https://doi.org/10.4161/cam.36224.

[43] T. Gebäck, M.M.P. Schulz, P. Koumoutsakos, M. Detmar, TScratch: a novel and simple software tool for automated analysis of monolayer wound healing assays, BioTechniques. 46 (2009) 265–274. https://doi.org/10.2144/000113083.

[44] M. Thommes, K. Kaneko, A.V. Neimark, J.P. Olivier, F. Rodríguez-Reinoso, J. Rouquerol, M. Thommes, Physisorption of gases, with special reference to the evaluation of surface area and pore size distribution (IUPAC Technical Report), Pac. 87 (2015) 1051. https://doi.org/10.1515/pac-2014-1117.

[45] N. Parker, M.J. Turk, E. Westrick, J.D. Lewis, P.S. Low, C.P. Leamon, Folate receptor expression in carcinomas and normal tissues determined by a quantitative radioligand binding assay, Analytical Biochemistry. 338 (2005) 284–293. https://doi.org/10.1016/j.ab.2004.12.026.

[46] J. Sudimack, R.J. Lee, Targeted drug delivery via the folate receptor, Advanced Drug Delivery Reviews. 41 (2000) 147–162. https://doi.org/10.1016/S0169-409X(99)00062-9.

[47] V. Horváth, O. Blanářová, L. Švihálková-Šindlerová, K. Souček, J. Hofmanová, P. Sova, A. Kroutil, P. Fedoročko, A. Kozubík, Platinum(IV) complex with adamantylamine overcomes intrinsic resistance to cisplatin in ovarian cancer cells, Gynecologic Oncology. 102 (2006) 32–40. https://doi.org/10.1016/j.ygyno.2005.11.016.

[48] J.-Q. Wang, J.-F. Kou, Z.-Z. Zhao, K.-Q. Qiu, H. Chao, Anthraquinone-bridged diruthenium(II) complexes inhibit migration and invasion of human hepatocarcinoma MHCC97-H cells, Inorg. Chem. Front. 4 (2017) 1003–1012. https://doi.org/10.1039/C7QI00149E.

[49] A. Gandalovičová, D. Rosel, M. Fernandes, P. Veselý, P. Heneberg, V. Čermák, L. Petruželka, S. Kumar, V. Sanz-Moreno, J. Brábek, Migrastatics—Anti-metastatic and Anti-invasion Drugs: Promises and Challenges, Trends in Cancer. 3 (2017) 391–406. https://doi.org/10.1016/j.trecan.2017.04.008.

[50] O. Veiseh, F.M. Kievit, R.G. Ellenbogen, M. Zhang, Cancer Cell Invasion: Treatment and Monitoring Opportunities in Nanomedicine, Advanced Drug Delivery Reviews. 63 (2011) 582–596. https://doi.org/10.1016/j.addr.2011.01.010.